OPEN ACCESS
IOP Publishing
Journal of Physics B: Atomic, Molecular and Optical Physics
J. Phys. B: At. Mol. Opt. Phys. **55** (2022) 095201 (7pp)
https://doi.org/10.1088/1361-6455/ac4ff2

Electron collision studies on the CH_2^+ molecular ion

K Chakrabarti[1], J Zs Mezei[2,3], I F Schneider[3] and J Tennyson[3,4,*]

[1] Department of Mathematics, Scottish Church College, 1 & 3 Urquhart Sq., Kolkata 700006, India
[2] Institute for Nuclear Research, 4001 Debrecen, Hungary
[3] LOMC-UMR6294 CNRS, Université Le Havre Normandie, 76058 Le Havre, France
[4] Department of Physics and Astronomy, University College London, Gower St., London WC1E 6BT, United Kingdom

E-mail: j.tennyson@ucl.ac.uk

Received 11 November 2021, revised 11 January 2022
Accepted for publication 28 January 2022
Published 5 May 2022

Abstract

Calculations are performed for electron collision with the methylene molecular ion CH_2^+ in its bent equilibrium geometry, with the goal of obtaining cross sections for electron impact excitation and dissociation. The polyatomic version of the UK molecular *R*-matrix codes was used to perform an initial configuration-interaction calculation on the doublet and quartet states of the CH_2^+ ion. Subsequently, scattering calculations are performed to obtain electron impact electronic excitation and dissociation cross sections and, additionally, the bound states of the CH_2 molecule and Feshbach resonances in the e-CH_2^+ system.

Keywords: hydrocarbons, electron impact excitation, electron impact dissociation, resonances, methylene, *R*-matrix

Supplementary material for this article is available online

(Some figures may appear in colour only in the online journal)

1. Introduction

Many low temperature plasma environments have hydrocarbon molecular ions as important constituents. Collision of electrons with molecules and their ions in these environments are important processes that play a fundamental role in initiating chemistry, particle balance and transport. For example, although the present tendency in the magnetically controlled International Thermonuclear Fusion Reactor type fusion devices is to coat the reactor walls with beryllium or tungsten, hydrocarbon ions, in particular the methylene ion CH_2^+, are found in the edge and divertor plasmas of fusion devices which operate with graphite as plasma facing material (McLean *et al* 2005). Another important context is that of the dusty plasmas, the CH_2 and CH_2^+ being species involved in the chain of reactions resulting in the growths of the nano and micro-particles. In these situations, the cross sections for different electron induced process are necessary to model the plasma flow (see for example Reiter and Janev (2010)), in particular electron impact dissociation and dissociative ionisation:

$$e + CH_2^+ \rightarrow \begin{cases} C^+ + H_2 + e \\ CH^+ + H + e \end{cases} \tag{1}$$

$$e + CH_2^+ \rightarrow \begin{cases} e + CH^+ + H^+ + e \\ e + C^+ + H^+ + H + e \\ e + C^+ + H_2{}^+ + e \\ e + C^+ + H^+ + H^+ + 2e \end{cases} \tag{2}$$

These processes, leading to the destruction of the CH_2^+ ions and to the C atom production (Janev and Reiter 2002a, Janev

* Author to whom any correspondence should be addressed.

and Reiter 2002b), are highly significant for understanding the carbon redeposition.

In the interstellar medium (ISM), CH_2^+ ions are synthesised in gas phase by collision of C^+ ions with hydrogen (Wakelam *et al* 2010) and through hydrogen abstraction by CH^+. On the other hand, CH_2^+ ions can be removed by reactions such as (1) and (2) and by dissociative recombination (DR),

$$e + CH_2^+ \rightarrow \begin{cases} C + H_2 \\ CH + H \\ C + H + H \end{cases} \quad (3)$$

which is known to proceed via Feshbach resonances (Larson *et al* 1998).

There is a considerable literature on CH_y^+ hydrocarbon ions, and CH_2^+ ions in particular, in the context of synthesis of hydrocarbons in the ISM (van Dishoeck *et al* 1996, van Dishoeck *et al* 2006, Wakelam *et al* 2010, Puglisi *et al* 2018, IdBarkach *et al* 2019). Significant work on CH_y^+ hydrocarbon ions have also been done relevant to plasmas for fusion (Janev and Reiter 2002a, Janev and Reiter 2002b, Vane *et al* 2007, Lecointre *et al* 2009, Reiter and Janev 2010). These works mainly focus on different electron impact cross sections relevant for plasma modeling.

Molecular structure calculations on CH_2^+ have been reported by several authors (Tennyson and Sutcliffe 1983, Theodorakopoulos and Petsalakis 1991, Kraemer *et al* 1994, Li *et al* 2015, Guo *et al* 2018, Ma *et al* 2021). Theodorakopoulos and Petsalakis (1991) obtained bending potential energy curves and vertical excitation energies (VEEs) of CH_2^+ for its bent C_{2v} and its linear $D_{\infty h}$ configurations. Accurate global potential energy surfaces (PES) were reported by Li *et al* (2015) and Guo *et al* (2018). Apart from these, there are also many spectroscopic studies on the rovibrational states of CH_2^+ (Rösslein *et al* 1992, Bunker *et al* 2001, Jensen *et al* 2002, Willitsch and Merkt 2003, Wang *et al* 2013).

In a number of earlier studies (Chakrabarti *et al* 2017, Chakrabarti *et al* 2018, Chakrabarti *et al* 2019, Ghosh *et al* 2020) we have studied electron collision with the CH molecule and its positive ion CH^+ in considerable detail. In these works, we not only computed cross sections for different electronic processes, but also identified many new neutral valence states of CH that are relevant for the DR. The present article aims to continue and extend our work to more complex hydrocarbon ions.

2. *R*-matrix calculations

2.1. R-matrix method

The *R*-matrix method, described in detail by Tennyson (2010) and Burke (2011), and its implementation in the polyatomic version of the UK molecular *R*-matrix codes (UKRmol) (Carr *et al* 2012) is used in the present work. The method employs a division of space into an inner region, a sphere of radius a (chosen to be $10a_0$ in this work) called the *R*-matrix sphere whose purpose is to include within it all short range interactions, and an outer region exterior to this sphere which contains all the long range interactions. This division allows the treatment of the short range and, the more complicated, long range interactions separately using different techniques (Tennyson 2010).

In the inner region, the wave function of the target (here CH_2^+) and a single continuum electron, together having $N+1$ electrons, is taken as

$$\Psi_k = \mathcal{A}\sum_{i,j} a_{i,j,k}\Phi_i(1,\ldots,N)F_{i,j}(N+1) + \sum_i b_{i,k}\chi_i(1,\ldots,N+1), \quad (4)$$

where $\mathcal{A}$ is an antisymmetrisation operator, $\Phi_i(1,\ldots,N)$ is the wave function of the N electron target and $F_{i,j}(N+1)$ are continuum orbitals. The functions $\chi_i(1,\ldots,N+1)$ in the last term are square integrable functions, called L^2 functions, are constructed by allowing the projectile electron to enter the target complete active space (CAS) and are included to take into account electron correlations and polarization of the target in presence of the projectile electrons. The coefficients $a_{i,j,k}$ and $b_{i,k}$ are obtained by diagonalizing the inner region Hamiltonian (Tennyson 1996).

The inner region wave function Ψ_k is then used with appropriate boundary conditions to obtain scattering information, the details of which are given in the following subsections.

2.2. Target calculations

We used the cc-pVTZ Gaussian basis sets (Pritchard *et al* 2019) centered on the C and H atoms to represent the target orbitals. These not only gave reasonably good target VEEs but also allows the inner region calculation to remain manageable with respect to computational resources.

The X $^2A_1$ ground state of CH_2^+ is known to be bent in C_{2v} symmetry and has the electronic configuration $(1a_1)^2(2a_1)^2(1b_2)^2(3a_1)^1$ (Pople and Curtiss 1987, Graber *et al* 1993). In this work all calculations are reported at the equilibrium C–H bond length $2.066a_0$ and the H–C–H bond angle 140.1° taken from Theodorakopoulos and Petsalakis (1991), which are very close to those obtained by more sophisticated coupled cluster calculations using large basis sets (Brinkmann *et al* 2002). An initial Hartree–Fock (HF) calculation was first performed on the X $^2A_1$ ground state of CH_2^+. The HF orbitals were then used in a configuration interaction (CI) calculation.

We considered two target models. In both models we kept two electrons frozen in the $1a_1$ orbitals while the remaining five electrons were distributed in the CAS. In the first model (M1), the CAS was defined by $(1a_1$–$6a_1, 1b_1$–$4b_1, 1b_2$–$4b_2)$, while in the second (M2) the CAS was chosen to be bigger with an additional $1a_2$ orbital, namely $(1a_1$–$8a_1, 1b_1$–$5b_1, 1b_2$–$5b_2, 1a_2)$. Table 1 shows the comparison of the VEEs form the X $^2A_1$ ground state of CH_2^+ to the first 12 low lying excited states. Although the second model M2 appears to produce VEEs slightly in better agreement with the theoretical results of Theodorakopoulos

Table 1. Comparison of the VEEs (in eV) from the X $^2A_1$ ground state to 12 low lying excited states of CH_2^+ for different target models. The target models used are the following:
M1: $(1a_1)^2(1a_1\text{–}6a_1, 1b_1\text{–}4b_1, 1b_2\text{–}4b_2)^5$
M2: $(1a_1)^2(1a_1\text{–}8a_1, 1b_1\text{–}5b_1, 1b_2\text{–}5b_2, 1a_2)^5$

Target state	M1	M2	Theory[a]	Theory[b]
X $^2A_1$	0[c]	0[d]	0[e]	0
1 $^2B_1$	0.92	0.81	0.84	0.83
1 $^4A_2$	5.24	5.07		
1 $^2A_2$	6.93	6.81	6.81	6.92
1 $^2B_2$	7.46	7.36	7.60	7.8
2 $^2A_2$	7.88	7.60	7.25	7.26
1 $^4B_1$	9.73	9.58		
2 $^2B_2$	9.48	9.17	9.25	9.6
2 $^2A_1$	11.17	10.50	10.44	11.1
3 $^2A_1$	13.52	13.04	12.81	
2 $^2B_1$	13.47	13.21	13.14	13.9
4 $^2A_1$	14.89	14.76	13.40	
3 $^2B_2$	13.22	13.23	13.53	

[a]Theodorakopoulos and Petsalakis (1991).
[b]Osmann *et al* (1999).
[c]Absolute energy −38.613 069 04 Hartree.
[d]Absolute energy −38.637 545 16 Hartree.
[e]Absolute energy −38.705 744 Hartree.

and Petsalakis (1991) and Osmann *et al* (1999), calculations with this model required much longer time compared to the model M1. We therefore chose the model M1 for subsequent calculations as it was computationally more efficient.

From table 1, we see that apart from the VEE of the 4 $^2A_1$ state, which appears too high compared to Theodorakopoulos and Petsalakis (1991), all other VEEs obtained by the target model M1 are in reasonably good agreement with the results of Theodorakopoulos and Petsalakis (1991) and Osmann *et al* (1999). Moreover, our dipole moment for the CH_2^+ ground state with model M1 is 0.701 D which compares perfectly with the value 0.701 D obtained by Brinkmann *et al* (2002) using coupled cluster calculation. The model M1 therefore provides a good description of the target for subsequent scattering calculations.

2.3. Scattering calculations

For the scattering calculations, we used $8a_1, 6b_1, 6b_2$ and $2a_2$ target orbitals allowing two virtual orbitals for each symmetry. Since the target CH_2^+ is a positive ion, the continuum functions were represented by Coulomb functions which were obtained as a solution of the radial Coulomb equation for an isotropic Coulomb potential, and the solutions with $l \leqslant 4$, and energy eigenvalue $\leqslant 5$ Ryd were retained in the calculation. The Coulomb functions were then fitted to GTOs using the procedure outlined in Faure *et al* (2002).

The target and continuum orbitals must all be orthogonal to each other. To ensure the orthogonality, the target and continuum orbitals were first individually Schmidt orthogonalized and finally the full set of target and continuum orbitals were symmetric orthogonalized, retaining only those orbitals for which the eigenvalue of their overlap matrix was less than a deletion threshold, chosen here to be 5×10^{-5}. The deletion

Table 2. Comparison of the VEEs (in eV) from the ground X $^3B_1$ state of CH_2 to some of its low lying excited states.

CH_2 state	This work	CI[a]	Romelt[b]	Yamaguchi[c]
X $^3B_1$	0.0[d]	0.0[e]	0.0[f]	0.0
1 $^1A_1$	1.16	0.995	1.14	
$^1B_1$	1.74	1.86	1.63	
2 $^1A_1$	3.24	3.31	3.38	
$^3A_1$	6.21	7.67	6.37	
$^3B_2$	7.35	8.05	7.59	7.86
$^1B_2$	7.25	9.25	7.63	7.75
$^3A_2$	7.63	7.47	7.57	7.23
$^1A_2$	8.33	8.39	8.46	

[a]CI calculation done at CH_2 equilibrium (C–H bond length 2.0314 a_0 and H–C–H bond angle 133.8°) using $(1a_1)^2\ (2a_1\text{–}6a_1, 1b_1\text{–}4b_1, 1b_2\text{–}4b_2)^6$ CAS-CI model.
[b]Römelt and Peyerimhoff (1981).
[c]Yamaguchi and Shaeffer (1997).
[d]Absolute energies of the ground state −38.985 233 Hartree.
[e]Absolute energies of the ground state −38.966 950 Hartree.
[f]Absolute energies of the ground state −39.060 34 Hartree.

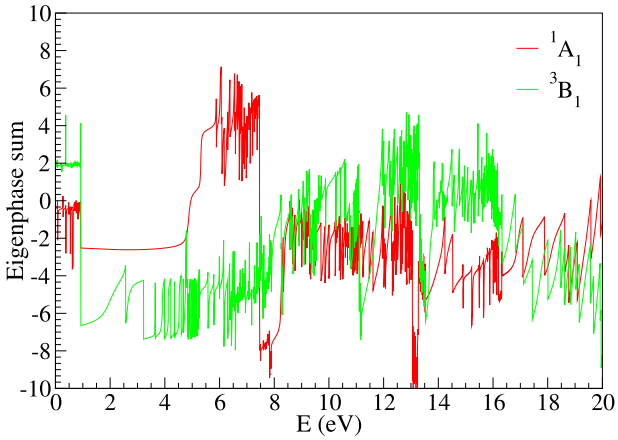

Figure 1. Eigenphase sums for the overall $e+$ CH_2^+ symmetries $^1A_1$ and $^3B_1$.

threshold depends on the *R*-matrix radius and was adjusted to ensure that there was no linear dependence.

An *R*-matrix was built at the boundary of the inner and outer region from the inner region solutions (equation (4)). The *R*-matrix were then propagated to an asymptotic distance $R_{asy} = 70a_0$ in a potential which included the Coulomb potential and the dipole and quadrupole potentials of the target, where they were then matched to asymptotic functions obtained from a Gailitis expansion (Noble and Nesbet 1984). This matching procedure yields the *K*-matrix from which all scattering observables can be obtained. A different route, however, is followed for obtaining bound states, as is outlined below.

For bound states, the *R*-matrix and wave functions were propagated using Runge–Kutta–Nystrom method (Zhang *et al* 2011) to an asymptotic distance $R_{asy} = 50a_0$ in a potential which included the Coulomb potential and the dipole and quadrupole potentials of target, and were matched to exponentially decreasing asymptotic functions (Noble and Nesbet 1984). A searching algorithm (Sarpal *et al* 1991) over a

Table 3. Resonance positions and widths (in Ryd) and effective quantum numbers at the CH_2^+ equilibrium for states of $^3B_1$ and $^1A_1$ symmetry of the e-CH_2^+ system below the first two CH_2^+ excited states. Numbers within brackets indicate power of 10.

Position	Width	ν	Position	Width	ν
		$^3B_1$ symmetry			
	Below 1^2B_1 state			Below $^4A_2$ state	
0.3558(−02)	0.2400(−04)	3.9466	0.1925	0.1075(−01)	2.2792
0.4870(−02)	0.5833(−04)	3.9875	0.2678	0.3334(−03)	2.9201
0.1567(−01)	0.4765(−04)	4.3815	0.2872	0.2789(−02)	3.1980
0.1718(−01)	0.6172(−04)	4.4465	0.3034	0.1910(−03)	3.5000
0.2685(−01)	0.1503(−04)	4.9440	0.3197	0.2426(−03)	3.9143
Position	Width	ν	Position	Width	ν
		$^1A_1$ symmetry			
	Below 1^2B_1 state			Below 1^2A_2 state	
0.2034(−01)	0.2198(−03)	4.5925	0.3582	0.9116(−02)	2.5716
0.3582(−01)	0.1225(−03)	5.5953	0.3907	0.2355(−02)	2.9015
0.4478(−01)	0.7510(−04)	6.5969	0.4323	0.1280(−02)	3.6009
0.5043(−01)	0.4929(−04)	7.5979	0.4424	0.2339(−02)	3.8615
0.5423(−01)	0.3407(−04)	8.5985	0.4492	0.3074(−02)	4.0762

non-linear quantum defect based grid (Rabadán and Tennyson 1996) was then used to find the bound states as roots of a determinant $\mathcal{B}(E)$ dependent on the energy. The details of the method are omitted and can be found in Sarpal *et al* (1991).

3. Results

All scattering calculations in this work were performed at a single geometry, namely the equilibrium geometry of the CH_2^+ target ion, for bound states of the CH_2 molecule, Feshbach resonances in the $e + CH_2^+$ system and cross sections for elastic scattering and electronic excitations. An 11 state scattering model including three $^2A_1$, three$^2B_1$, three$^2B_1$ and two $^2A_2$ target states in the close coupling expansion equation (4) were used for the singlet $e + CH_2^+$ scattering close-coupling expansion, while a 15 state model which included the same 11 doublet states as in the singlet state model, together with the lowest each of the $^4A_1$,$^4B_1$,$^4B_2$, and $^4A_2$ states was used in equation (4) for triplet symmetry close-coupling expansion. As will be shown below, this procedure provides a reliable scattering model which was tested by calculating the bound states of CH_2.

3.1. Bound states

Table 2 shows the VEEs for the bound states of CH_2 from its X $^3B_1$ ground state to few of its low lying excited states. For a comparison, we also did a quantum chemistry-style CI calculation on CH_2 at its equilibrium geometry (C–H bond length 2.0314 a_0 and H–C–H bond angle 133.8°) using a $(1a_1)^2$ $(2–6a_1, 1–4b_1, 1–4b_2)^6$ CAS-CI model. The VEEs are then compared with the multi reference double excitation calculation of Römelt and Peyerimhoff (1981) and the coupled cluster results of Yamaguchi and Shaeffer (1997). From table 2, it is clear that the VEEs obtained by the R-matrix method are in very good agreement with all others. The fact that the calculated bound state energies are consistent and accurate enough indicates that our scattering model is reasonably good.

3.2. Resonances at equilibrium

For resonance calculation, the R-matrix was propagated to 70 a_0. Resonances were detected by the characteristic change in sign of the second derivative of the eigenphase sum $\delta(E)$ given by

$$\delta(E) = \sum_i \arctan(K_{ii}), \tag{5}$$

where K_{ii} are the elements of the diagonalised K matrix. They were then fitted to a Breit–Wigner profile (Tennyson and Noble 1984) with an energy grid 0.005 eV to obtain the resonance energy E and width Γ.

Figure 1 shows the plot of two typical eigenphase sums for $^1A_1$ and $^3B_1$ symmetries. Characteristic of electron collision with ions, the figure shows numerous resonances some of which are tabulated in table 3 according to their parent state. As seen from the table, many of the resonances appear to be in Rydberg series which can be identified by their effective quantum numbers. The relatively small gap between the ground and first excited electronic state means that the resonances start with relatively high effective quantum numbers, $\nu \approx 4$, and then closely space.

A full set of fits to the resonances covering all overall scattering symmetries is given in the supplementary material (https://stacks.iop.org/JPB/55/095201/mmedia).

3.3. Electron impact excitation

Our calculated cross sections for electron impact excitation of CH_2^+ from the ground state to four of its lowest doublet states are shown in figure 2. As in the elastic cross section,

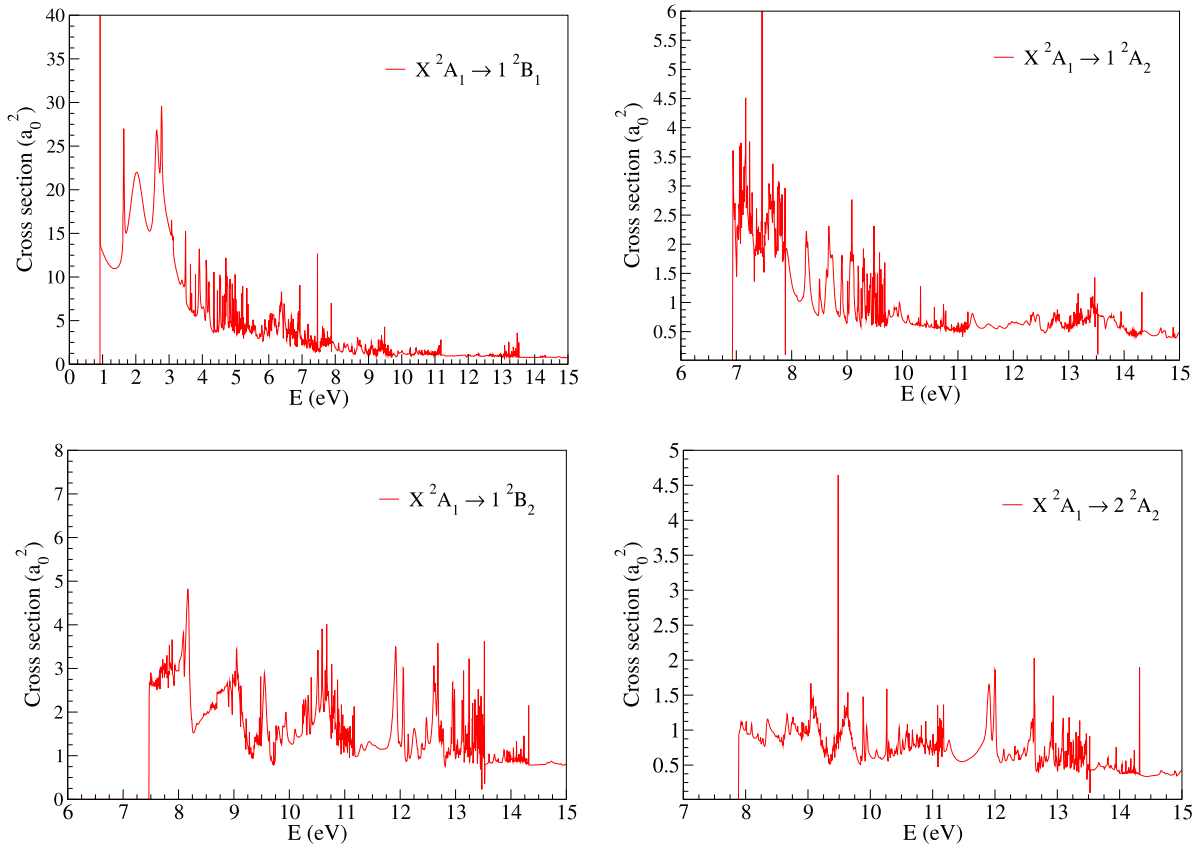

Figure 2. Cross sections for electronic excitation form the X^2A_1 ground state to the first four excited states of doublet symmetry as given in table 1 and indicated in each panel.

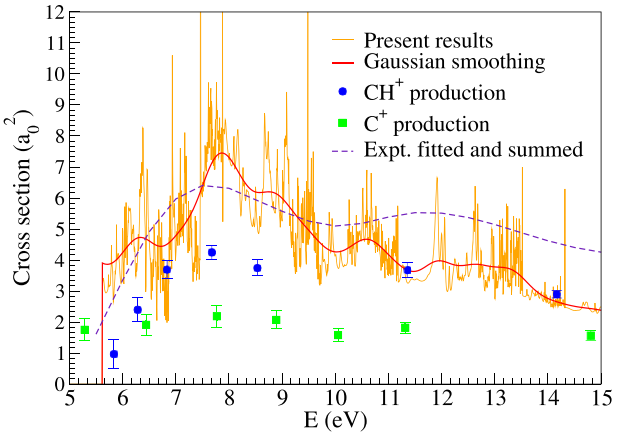

Figure 3. Cross section for the electron impact dissociation of the CH_2^+ ion. Thin curve: present *R*-matrix results (see text). Thick (red) curve: present result after smoothing with a Gaussian function. Green circles with error bars: experimental results for C^+ ion production Vane *et al* (2007). Blue circles with error bars: experimental results for CH^+ ion production Vane *et al* (2007). Dashed curve: experimental results for C^+ and CH^+ ion production summed after suitable fitting (see text).

the excitation cross sections show highly resonant behaviour due to temporary captures into resonant states. Particularly, the X $^2A_1 \rightarrow 1^2B_1$ excitation cross section shows evidence of a large resonance near threshold. Referring to figure 1, this is likely due to the large $^3B_1$ resonance near 1 eV as seen from the plot of the $^3B_1$ eigenphase sum. Generally, the excitation cross sections decrease with increasing incident energy and the cross sections from the higher lying excited states are much smaller.

Our calculations only consider partial waves with $l \leqslant 4$. For dipole allowed electronic excitation processes it is known that higher l partial waves contribute to the electronic excitation and for electron collisions with neutral targets allowance for this is often made using the Born approximation; a standard procedure exists for this within the UKRMol codes (Kaur *et al* 2008). Considering the low-lying states of CH_2^+ excitation the two low-lying $^2A_2$ states are dipole forbidden but the 1 $^2B_1$ and 1 $^2B_2$ are both connected to the ground state by dipoles in the region of 1 a.u.. Test calculations showed that allowing for this approximately led to a small increase in the 1 $^2B_2$ cross section but a very large increase in the predicted electronic excitation cross section for the 1 $^2B_1$. However, the 1 $^2B_1$ state has a very low excitation threshold meaning it will be excited by slow-moving electrons and that under these circumstances it is necessary to consider the rotational motion of the target which will lead a reduction in effect of the long-range dipole. Treatment of this will require further developments and is left to future work. However, neglect of the partial waves with $l > 4$ means that our predicted 1 $^2B_1$ and 1 $^2B_2$ cross sections, and the dissociation cross sections given below, are probably too low.

3.4. Electron impact dissociation

Experimental cross sections for electron impact dissociation were obtained by Vane *et al* (2007) for the production of CH^+ and C^+ fragments. Although model calculations exist for the electron impact dissociation of CH_2^+ ions (see for example Reiter and Janev (2010)), to the best of our knowledge, the 2007 experiments have never been described by any *ab initio* calculation.

The dissociation of CH_2^+ into the lowest dissociation channels, namely $e + CH^+ + H$ and $e + C^+ + H_2$, proceed via direct dissociative excitation and have thresholds 6.08 eV and 5.62 eV respectively (Vane *et al* 2007). In deriving the dissociation cross section, we assumed that electronic excitations to all states above the respective dissociation thresholds lead to dissociation. In our calculation, we have included the states $1\ ^2B_1$, $1\ ^2B_2$, $1\ ^2A_2$, and the $2\ ^2A_2$ excited states all of which lie close to one another at the CH_2^+ equilibrium. Moreover, except the $1\ ^2B_1$ state, which has both valence and Rydberg character, all the other three are of valence character at equilibrium (see for example (Theodorakopoulos and Petsalakis 1991)) and hence are likely to dissociate to the $e + C^+ + H_2$ (5.62 eV) or the $e + CH^+ + H$ (6.08 eV) dissociation limits, which are the most relevant in the energy range considered. Since the dissociation channels cannot be separated in our calculations, our cross section in figure 3 represents a sum over these channels. For better comparison, we have also shown our cross sections after smoothing by using a Gaussian function. The experimental data from Vane *et al* (2007) are available for each of the dissociation channels mentioned above. The energy grid of the experimental cross sections for these two dissociation channels, however, are neither the same nor uniform. Therefore, to sum the experimental data, we first spline interpolated each set over the same and uniform energy grid. This allowed us to sum the cross section for the experimental data. In figure 3, this sum is shown as the dashed line and it agrees fairly well with our computed cross section. In particular, the peak near 8 eV agrees quite well with the spline interpolated summed experimental curve. However, we note that since the experimental data is non uniformly spaced, the interpolated curve may not always reflect the actual trend. For example, we suspect the agreement of the interpolated curve with our calculation would have been much better between 11 eV–15 eV had there been more experimental points available in this region. Similarly, below 6 eV, the interpolated experimental curve appears to diverge for our Gaussian fitted curve. This is a result of the fitting procedure, the interpolated experimental curve actually follows the trend of our raw cross section curve.

4. Conclusion

As mentioned in the introduction, CH_2^+ is a very important constituent in low temperature plasma environments. However, despite its importance, electron collisions studies on CH_2^+ have been rare. In fact, we could not find any *ab initio* calculation for the cross sections included in the present work. The only cross section result available, seems to be the total ionisation cross section of CH_2^+ calculated within the binary-encounter-Bethe model by Irikura *et al* (2002).

In this work, we have presented a reliable set of cross sections for the electronic excitation, and electron impact dissociation of the CH_2^+ ion. In fact, none of these cross sections have ever been reported before by any *ab initio* calculation. Additionally, we have also calculated and have given the position and width for some of the Feshbach resonances in the e-CH_2^+ system. These Feshbach resonances, as is well known, are the routes to DR of the CH_2^+ ion. However, its treatment requires a more comprehensive calculation of the resonance energies, widths and the PES of the CH_2^+ and CH_2 states. This is the subject of an ongoing project.

Acknowledgments

The authors acknowledge support from Fédération de Recherche Fusion par Confinement Magétique (CNRS, CEA and Eurofusion), La Région Normandie, FEDER and LabEx EMC3 via the Projects PTOLEMEE, Bioengine, the Institute for Energy, Propulsion and Environment (FR-IEPE), and ERASMUS-plus conventions between Université Le Havre Normandie and University College London. We are indebted to Agence Nationale de la Recherche (ANR) via the project MONA, Centre National de la Recherche Scientifique via the Programme National 'Physique et Chimie du Milieu Interstellaire' (PCMI). JZ thanks the financial support of the National Research, Development and Innovation Fund of Hungary (NKFIH), under the K18 and FK19 funding schemes with Project Nos. K128621 and FK132989. JZ and IFS are grateful for the support of the NKFIH-2019-2.1.11-TÉT-2020-00100 and Campus France-Programme Hubert Curien+BALATON+46909PM Projects.

ORCID iDs

K Chakrabarti https://orcid.org/0000-0003-0013-5610
J Zs Mezei https://orcid.org/0000-0002-7223-5787
I F Schneider https://orcid.org/0000-0002-4379-1768
J Tennyson https://orcid.org/0000-0002-4994-5238

References

Brinkmann N R, Richardson N A, Wesolowski S S, Yamaguchi Y and Schaefer H F III 2002 *Chem. Phys. Lett.* **352** 505
Bunker P R, Chan M C, Kraemer W P and Jensen P 2001 *Chem. Phys. Lett.* **341** 358
Burke P G 2011 *R-Matrix Theory of Atomic Collisions* (Heidelberg: Springer)
Carr J M *et al* 2012 *Eur. Phys. J.* D **66** 58
Chakrabarti K, Dora A, Ghosh R, Choudhury B S and Tennyson J 2017 *J. Phys. B: At. Mol. Opt. Phys.* **50** 175202
Chakrabarti K, Ghosh R and Choudhury B S 2019 *J. Phys. B: At. Mol. Opt. Phys.* **52** 105205
Chakrabarti K, Mezei J Z, Motapon O, Faure A, Dulieu O, Hassouni K and Schneider I F 2018 *J. Phys. B: At. Mol. Opt. Phys.* **51** 104002
Faure A, Gorfinkiel J D, Morgan L A and Tennyson J 2002 *Comput. Phys. Commun.* **144** 224

Ghosh R, Chakrabarti K and Choudhury B S 2020 *Plasma Sources Sci. Technol.* **29** 095016
Graber T, Kanter E P, Vager Z and Zajfman D 1993 *J. Chem. Phys.* **98** 7725
Guo L, Ma H, Zhang L, Song Y and Li Y 2018 *RSC Adv.* **8** 13635
Ma H, Zhang C, Song Y, Ma F and Li Y 2021 *J. Phys. Chem.* A **125** 5490
IdBarkach T, Chabot M, Béroff K, Della Negra S, Lesrel J, Geslin F, Le Padellec A, Mahajan T and Díaz-Tendero S 2019 *Astron. Astrophys.* **628** A75
Irikura K K, Kim Y K and Ali M A 2002 *J. Res. Natl Inst. Stand. Technol.* **107** 63
Janev R K and Reiter D 2002a *Phys. Plasmas* **9** 4071
Janev R K and Reiter D 2002b *Collision Processes of Hydrocarbon Species in Hydrogen Plasmas: I. The Methane Family* (Jülich: Forschungszentrum-Jülich)
Jensen P, Wesolowski S S, Brinkmann N R, Richardson N A, Yamaguchi Y, Schaefer H F and Bunke P 2002 *J. Mol. Spectrosc.* **211** 257
Kaur S, Baluja K L and Tennyson J 2008 *Phys. Rev.* A **77** 032718
Kraemer W P, Jensen P and Bunker P R 1994 *Can. J. Phys.* **72** 871
Larson A *et al* 1998 *Astrophys. J.* **505** 459
Lecointre J, Belic D S, Jureta J J, Janev R K and Defrance P 2009 *Eur. Phys. J.* D **55** 569
Li Y Q, Zhang P Y and Han K L 2015 *J. Chem. Phys.* **142** 124302
McLean A G *et al* 2005 *J. Nucl. Mater.* **337–339** 124–8
Noble C J and Nesbet R K 1984 *Comput. Phys. Commun.* **33** 399
Osmann G, Bunker P R, Kraemer W P and Jensen P 1999 *Chem. Phys. Lett.* **309** 299
Pople J A and Curtiss L A 1987 *J. Phys. Chem.* **91** 155
Pritchard B P, Altarawy D, Didier B, Gibson T D and Windus T L 2019 *J. Chem. Inf. Model.* **59** 4814
Puglisi A, Miteva T, Kennedy E T, Mosnier J-P, Bizau J-M, Cubaynes D, Sisourat N and Carniato S 2018 *Phys. Chem. Chem. Phys.* **20** 4415
Rabadán I and Tennyson J 1996 *J. Phys. B: At. Mol. Opt. Phys.* **29** 3747–61
Reiter D and Janev R K 2010 *Contrib. Plasma Phys.* **50** 986
Römelt J, Peyerimhoff S D and Buenker R J 1981 *Chem. Phys.* **54** 147
Rösslein M, Gabrys C M, Jagod M-F and Oka T 1992 *J. Mol. Spectrosc.* **153** 738
Sarpal B K, Branchett S E, Tennyson J and Morgan L A 1991 *J. Phys. B: At. Mol. Opt. Phys.* **24** 3685–99
Tennyson J 1996 *J. Phys. B: At. Mol. Opt. Phys.* **29** 1817–28
Tennyson J 2010 *Phys. Rep.* **491** 29–76
Tennyson J and Noble C J 1984 *Comput. Phys. Commun.* **33** 421
Tennyson J and Sutcliffe B T 1983 *J. Mol. Spectrosc.* **101** 71
Theodorakopoulos G and Petsalakis I D 1991 *J. Mol. Struct.* **230** 205
van Dishoeck E F, Bearda R A and van Hemert M C 1996 *Astron. Astrophys.* **307** 645
van Dishoeck E F, Jonkheid B and van Hemert M C 2006 *Faraday Discuss.* **133** 231
Vane C R, Bahati E M, Bannister M E and Thomas R D 2007 *Phys. Rev.* A **75** 052715
Wakelam V *et al* 2010 *Space Sci. Rev.* **156** 13
Wang H, Neese C F, Morong C P, Kleshcheva M and Oka T 2013 *J. Phys. Chem.* A **117** 9908
Willitsch S and Merkt F 2003 *J. Chem. Phys.* **118** 2235
Yamaguchi Y and Shaeffer H F III 1997 *J. Chem. Phys.* **106** 1819
Zhang R, Baluja K L, Franz J and Tennyson J 2011 *J. Phys. B: At. Mol. Opt. Phys.* **44** 035203